ICANS XIX,
19th meeting on Collaboration of Advanced Neutron Sources
March 8 – 12, 2010
Grindelwald, Switzerland

A Study of Proton Beam Profile on the Target at JSNS

Shin-ichiro MEIGO, Motoki OOI, Manabu ITO, Shinichi SAKAMOTO
and Masatoshi FUTAKAWA
J-PARC Center, JAEA
Tokai, Ibaraki, 319-1195, Japan

ABSTRACT

At J-PARC, 3-GeV proton beam with repetition of 25 Hz is introduced to the neutron target of JSNS. After November 2010, JSNS succeeded to perform stable operation with a power of 120 kW. In order to obtain beam properties, we measured the beam size by using the profile monitors. From the results of beam width measurements, the beam emittance and twiss parameter are obtained by fitting result along beam directions. It is found that the design calculation shows good agreement with experimental result. Since the muon production target is located upstream of neutron production target, beam scattering in the muon target increases the size and emittance of the beam. The effect due to the scattering was measured by the comparison of the beam sizes with and without the muon production target. In order to obtain actual beam profile on the target, a new technique was developed utilizing an Imaging Plate(IP). It is recognized that the beam width obtained by IP are in good agreement with the result by Multi-Wire Profile Monitor(MWPM).

1. Introduction

In the Japan Proton Accelerator Research Complex (J-PARC)[1], a MW-class pulsed neutron source, the Japan Spallation Neutron Source (JSNS)[2], and the Muon Science facility (MUSE)[3] were installed in the Materials and Life Science Experimental Facility (MLF) shown in Fig. 1. The 3-GeV proton beam is introduced to the mercury target for a neutron source and to a carbon graphite target with thickness of 20-mm thickness for a muon source. In order to utilize the proton beam efficiently for particle productions, both targets are aligned in a cascade scheme, where the graphite target is located 33 m upstream of the neutron target.

For both sources the 3-GeV proton beam is delivered from a rapid cycling synchrotron (RCS) to the targets. Before injection to the RCS, the proton beam is accelerated up to 181 MeV by a LINAC. The beam is accumulated in short bunches of less than 100 ns duration and accelerated up to 3 GeV in the RCS. After extraction, the 3-GeV proton beam is transferred to the muon production target and the spallation neutron source.

Recently it became evident that pitting damage appears in the target container of the mercury target[4]. Several facilities are studying the effect; Alternating Gradient Synchrotron(AGS) and Weapon Neutron Research facility(WNR) are pursuing off-beam experiments[5]. It has been reported that the damage is proportional to the 4th power of the beam peak current density[5]. Beam profile monitoring plays an important role in comprehending the damage to the target. It is necessary to know the characteristics of the projectile beam on the target.

Due to the pitting damage, beam properties such as beam profile and peak current density on the target are indispensable. In order to obtain the beam profile on the target

in early stage of the beam commissioning, we performed a foil activation technique[6] in which the residual dose distribution was measured on an aluminium foil placed in front of the target. The result given by the foil activation technique gives good agreement with the result by Multi-Wire Profile Monitor(MWPM). However, it is impossible to perform the same activation technique again because the residual does on the target is extreme high such as 1 Sv/h. Therefore, a new technique is required to measure the beam profile on the target.

In general, especially for the high power accelerator facilities such as J-PARC, proton beam characteristics are important. At J-PARC, beam transport line plays role of beam analyzer for 3-GeV protons extracted from the RCS. At the MLF, the effect due to the muon production target is indispensable, especially for the beam scattering. In this study, the beam emittance and twiss parameter were measured. Also the effect of beam scattering on the muon production target was also measured.

2. Proton beam monitors

The details of the monitor are described in Ref[6]. Here, the monitors are briefly described. To measure the beam intensity, Current Transformers (CTs) are installed in the beam line. Inside the current transformers, a titanium duct is attached for connection to other vacuum equipment. To measure the beam position and shape, Multi-Wire Profile Monitors (MWPMs) are installed in the beam line. Silicon Carbide (SiC) is utilized as sensor wires due to their small interaction with the primary beam. The wire frame can be moved out so that the beam can pass without interaction when no measurement is performed. A stationary type of beam profile monitor was located at the proton beam window shown in Fig. 1. The proton beam window is located at 1.8 m upstream of the neutron target, which consists of aluminium alloy of (AlMg3) having thickness of 5 mm in total. In order to recognize beam profile on the muon production target, a movable profile monitor is placed.

In order to watch the beam center position without interaction, Beam Position Monitors (BPMs) are installed. Beam position monitors consist of quadruple electrodes. The position of the beam is measured by the induction of wall currents in the electrode. The center position of the beam can be obtained by the difference among the pulse height of signals.

3. Measurement of beam profile on the mercury target

3.1 Activation technique by imaging plate

In order to perform beam profile measurement by activation, access to the target is necessary after beam irradiation. The radiation around the target is extremely high such as several Sv/h therefore a remote handling technique is required. We have developed an activation technique by utilizing an Imaging Plate(IP). By remote handling technique, an IP(Fuji Film BAS-SR 2040) is attached to the target vessel shown in Fig. 1. The IP contained in holder was attached to the hook of in-cell crane by human hands. At the entrance of hot cell, radiation was several tenth of μSv/h so that human can access. The IP approached to the target by the crane and contacted with the target by help of the master slave manipulator as shown in Fig. 1. Typical duration of exposure time was 5 min. After the exposure, the image of radiation was read out by the reader of the IP.

In Fig. 2, the beam profile result obtained by the IP after 120 kW beam irradiation in December 2009 is shown. In the distribution, it was recognized that a clear Gaussian peak exists without tilting, which showed the similar result by foil activation technique[6]. Figure 2 also shows the horizontal distribution obtained by the IP. The distribution can be well described by the combinations of two Gaussian functions having small and large widths. The shorter one was thought to be the initial protons. The longer was thought to be the secondary particles.

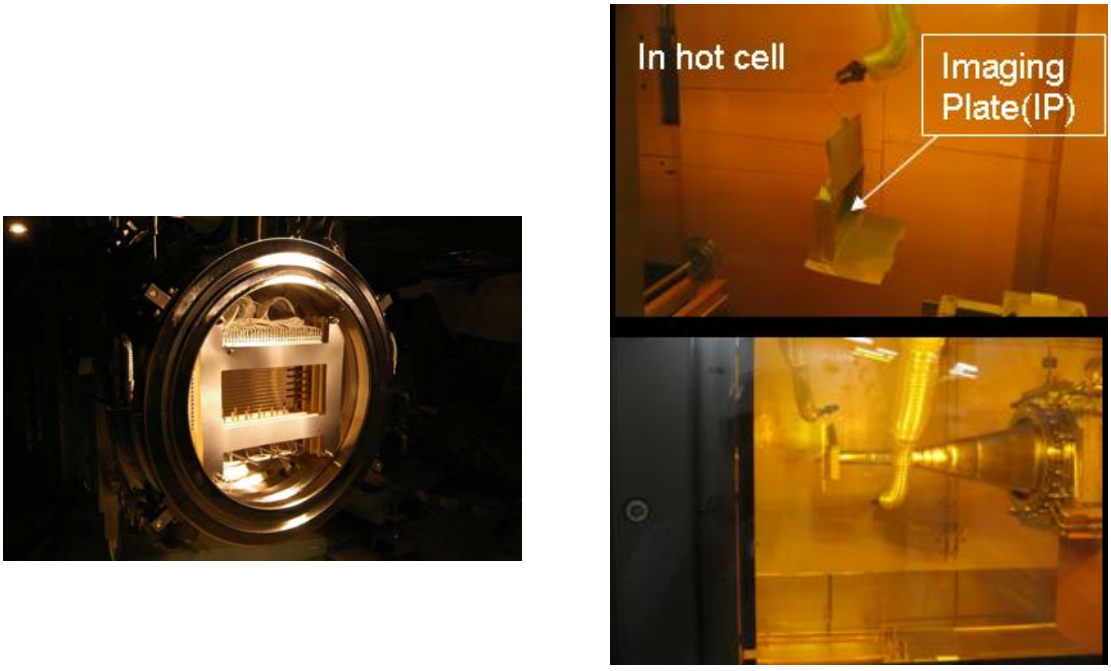

Fig. 1: Multi-Wire Profile Monitor (MWPM) located on the proton beam window(left) and activation technique using Imaging Plate (IP) located on the target vessel performed after irradiation at hot cell of the MLF(right).

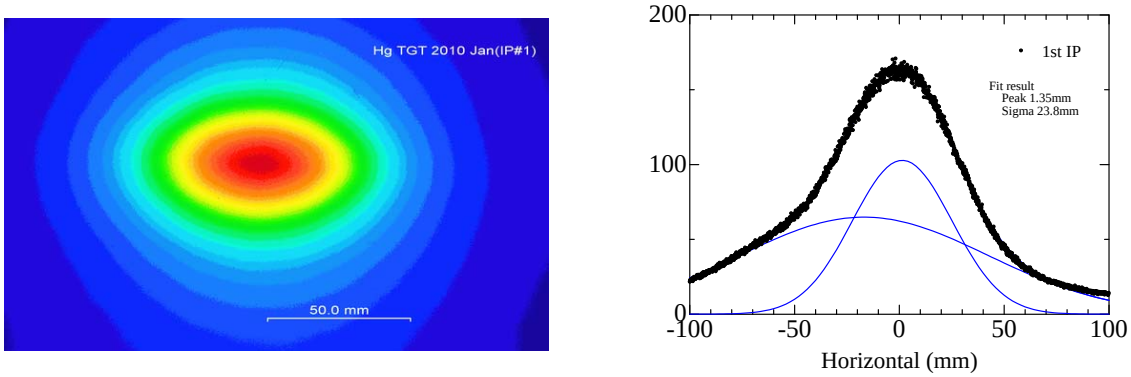

Fig. 2: Result of beam profile obtained by activation technique. 2D profile(left) and profile in horizontal direction with fitting Gaussian function(right).

3.2 Profile obtained by MWPM

During beam operation, beam profile was continuously measured by the MWPM located on the proton beam window. The result of the profile is shown in Fig. 3. For each pulse, Gaussian function fitting was performed to obtain peak heat density. Beam profile

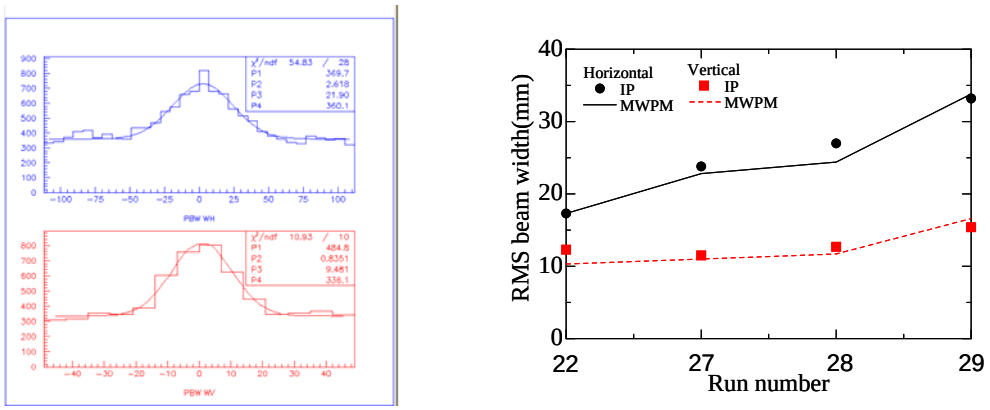

Fig. 3: Result of beam profile obtained by MWPM located on the proton beam window(left) and comparison of beam profile result at the target obtained by MWPM and activation technique(right). The width by IP are shown as circles and square for horizontal and vertical directions, respectively. The width by MWPM is shown as solid and dotted lines for horizontal and vertical directions, respectively.

on the target is slightly different from the profile on the MWPM, because of the beam divergence. In order to obtain the beam profile on the target, the beam width is expanded about 20% on the MWPM to correct the width for the divergence of the beam.

3.3 Comparison of beam profile results on the target

Figure 3 also shows the results of beam width obtained by the IP and the MWPM for each run. As the beam power increased, we expanded gradually the beam size. In each run,

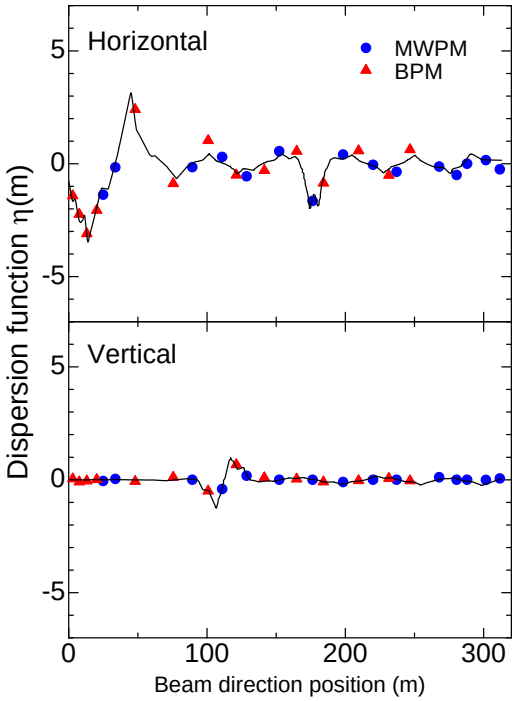

Fig. 4: Results of dispersion functions in horizontal and vertical directions by measuring the beam shifts with MWPM(circle) and BPM(triangle) when momentum is changed. Calculation result (solid line) is also shown.

it was found that the results obtained by the IP and the MWPM showed good agreement. Therefore, we can obtain a reliable beam profile on the mercury target from the MWPM. It should be noted that the muon production target is placed in the beam position during long period for users beam supply. Result of IP in Fig. 3 includes the effect of the scattering in the muon target.

4. Measurement of beam optics parameter

4.1 Dispersion function

By changing the beam momentum, beam position is shifted as the dispersion function. From the shift of the beam position, we tried to obtain the dispersion function. In the measurement, by changing RF in the RCS, the beam momentum was shifted ±0.4% from the nominal momentum of 3 GeV. The dispersion function can be obtained from the shift of beam position divided by the momentum difference. Figure 4 shows the experimental results compared with calculation result. It was found that the design calculation showed good agreement with the experiment. We designed the dispersion free beam transport line and could demonstrate it.

4.2 Beam emittance and twiss parameter

From the results of the MWPMs existing 15 pieces along beam line, the beam width distribution was obtained. Assuming the beam optics to be designed, we obtained the beam emittance and twiss parameter by fitting of the beam width distribution. With free emittance and twiss parameters of α and β, the whole distribution was fitted by the TRANSPORT code.

In Fig. 5, the beam width distribution, which is standard deviation obtained by fitting Gaussian function, is shown for the beam power of 120 and 300 kW with horizontal and vertical tunes of the RCS of (6.42, 6.42) having injection painting area of 150 π mm·mrad. In table 1, the results of beam emittance are shown. It was found that, as increase of beam power, the beam emittance increased. This fact is mainly caused by the space charge effect in the accelerator. In table 1, the result of beam emittance calculation for 300 kW is shown, which is given by the accelerator team. It is recognized that the calculation gives good agreement with the experiment. Also twiss parameters obtained by the present method are shown in table 2. Although slight differences exist, the calculation shows good agreement with experiment.

Table1.: Beam emittance obtained by the fitting of beam radius distribution by MWPMs

Beam power(kW)	ε_h(πmm mrad)	ε_v(πmm mrad)	Calc(πmm mrad)
120	2.7	2.7	
300	5.3	4.9	5.4

Table2.: Twiss parameter for beam power of 300 kW

	Experiment α	Experiment β(m)	Calculation α	Calculation β(m)
Horizontal	-1.84	20.4	-2.35	24.8
Vertical	0.57	5.28	0.89	5.88

5. Effect of muon production target

5.1 Beam transmission rate due to muon production target

The muon production target causes beam loss. The radiation caused by the muon production target can be measured by the beam loss monitors located several meters upstream of the muon target. In order to observe beam transmission rate, we measured difference of beam intensities by the CT located downstream of the target with and without muon target. It is found that the experimental result of transmission is 93.1% and calculation gives 94%. The calculation shows good agreement with the experiment. It is recognized that the calculation gives reliable result on to the beam loss effect due to the muon production target.

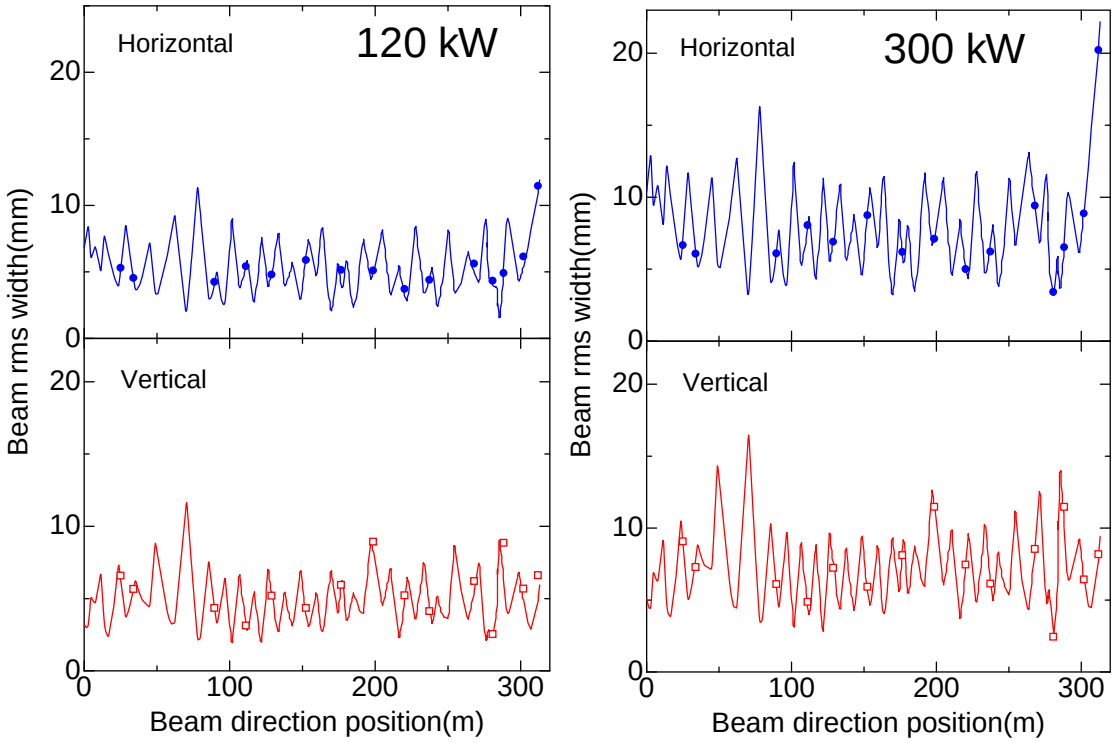

Fig. 5: Beam profile measurements for horizontal(upper) and vertical(lower) directions obtained by MWPM and fitting results utilizing free twiss parameter and emittance. Results for 120 and 300 kW are shown on left-hand side and right-hand side, respectively.

5.2 Effect of the beam scattering due to muon production target

At the MWPM located at the proton beam windows, effect on the beam properties due to the muon production target was measured, which is shown in Table 3. The original beam optics has the beam waist at the muon target. Because of the request of muon team, beam optics was changed to decrease the peak heat density at the muon target. The size ob the beam could be expanded, however, it is failed to have beam waist at the muon target because of lack of study time. From the results in Table 3, it was found that the blow-up of emittance is quite different in the both case. In the case of waist at the target, the

emittances slightly increase as ~10 %, which is relatively small. For the optics without waist at the target, the blow up of emittance becomes relatively large. From the measurement, it was recognized that the peak current density on the mercury target decrees 19% and 52 % due to the muon target for the beam optics with and without beam waist, respectively. Without beam waist, the peak density on the mercury target is significantly decreased due to the scattering at the muon production target.

In Table 3, it should be noted that the tune of the RCS is slightly difference. In upper case in Table 3 with waist, previous horizontal and vertical tunes of (6.40, 6.42) was used and in lower case the latest tunes of (6.42, 6.42) was used, which had same tune the result shown in left-hand side Fig. 5. In Table 3, beam painting area for injection at the RCS was different as well. Without the muon target, the emittance of upper case is larger than the emittance of lower case. Due to the scattering at the muon target, small painting injection has larger emittance than the large painting area.

Table3.: Effect on beam emittance due to the scattering of muon production target (all unit in π mm mrad)

Beam optics at muon target	RCS painting area	W/o Target ε_h	W/o Target ε_v	W/ Target ε_h	W/ Target ε_v
With beam waist	Large	3.9	3.5	4.2	4.2
Without beam waist	Small	2.7	2.7	8.0	4.0

6. Peak heat deposition

6.1 Present peak heat deposition

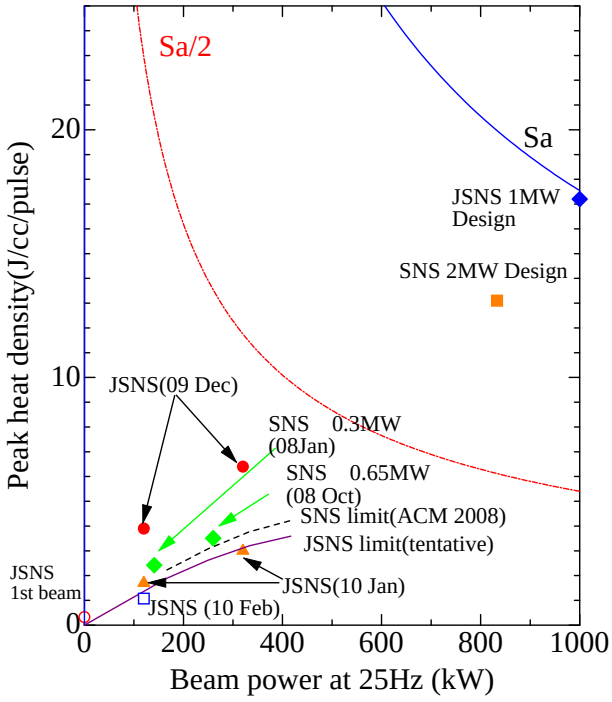

Fig. 6: Relationship between beam power at 25-Hz operation and peak heat density in the mercury target. Sa is allowable stress for fatigue of target vessel. JSNS Present results(circle and triangle) and SNS results(green diamond) are shown. Operational limit at SNS(dashed curve) and JSNS tentative limit(solid curve) are also shown. Sa/2 had been utilized limit before pinhole were found at SNS.

In Fig. 6, relationship between the beam power with 25 Hz and the peak heat deposition density in the target is shown. In early stage of beam commissioning, we had determined to keep the peak heat smaller than half of the Sa, which is allowable stress for fatigue of target vessel.

Recently, a pinhole is found recently at SNS target vessel. By concerning the present status of storage yard for waste such as target vessel and preparation for the new target vessel having helium babble injection to mitigation pressure wave, we determined to decrease the chance to have pinhole before receiving new target vessel. SNS has kept limitation curve shown in Fig. 6. Therefore, we determined new criteria as 75 % of SNS limit. By expanding beam by tuning of last 4 set of quadrupole magnets located at downstream, the actual density becomes smaller than our new criteria.

6.2 Peak heat deposition at 1-MW operation

As beam was expanded, the heat generation in the vicinities of the target becomes higher. We determined that heat deposition in the vicinities to be kept smaller than 1 W/cc. By conserving the aspect ratio of horizontal beam width to vertical to be 2.22, the heat deposition in vicinities is calculated. In Fig. 7, the relationship between the heat deposition in the vicinities and peak heat deposition in the center of mercury target is shown. It is recognized that the allowable heat deposition can be achieved by expanding the beam at 1-MW operation. Since it is difficult to predict the intensity of beam halo, it is better to utilize octupole magnets to decrease the peak density. At peripheral parts, we have many thermocouples to watch the actual heat deposition. By watching the temperatures, the

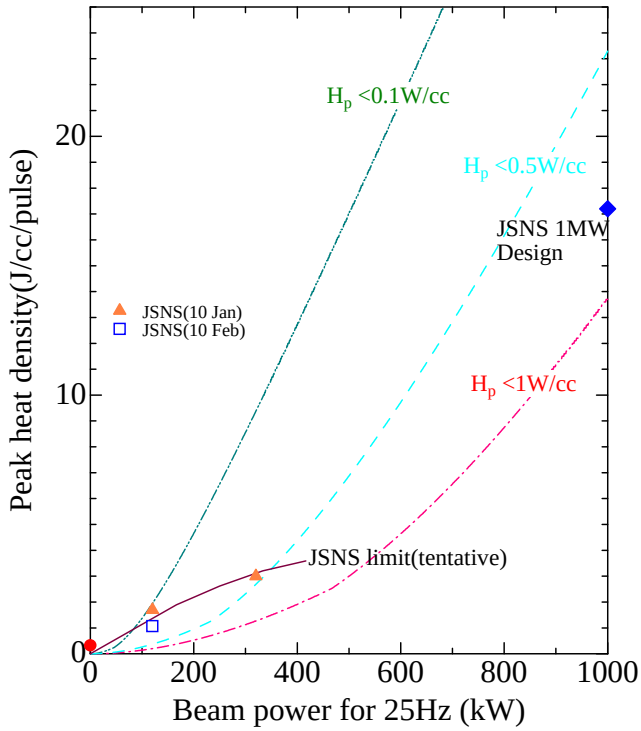

Fig. 7: For the heat depositions in the vicinities of 0.1, 0.5 and 1W/cc, peak heat densities in the target are shown as dashed double-dotted curvet, dashed curve and dashed dotted curve, respectively.

beam will be gradually expanded keeping low heat deposition at peripheral parts.

7. Summary

In order to measure the beam profile on the mercury target, a new technique has been developed utilizing the IP and remote handling technique. The beam profile result obtained by IP shows good agreement with the result by the MWPM. Reliable peak density of the proton beam can be obtained. We have measured beam properties and the effect due to the muon production target. It is found that beam properties show good agreement with calculation. The beam emittance blow-up is depending on the beam optics on the muon target. The peak density decrees 51 % due to the scattering for the beam optics without beam waist at the muon target. In this beam optics, beam operation should be paid attention for the drastically change of peak density on the mercury target.

In order to decrease the peak density and avoid pitting damage on the target, we tried to expand to have small peak density. From the present results, we estimated the peak density on the target in the future operation. It is recognized that peak during 1 MW operation is smaller than the allowable value, that is heat deposition less than 1 W/cc in target vicinities.

References

1. The Joint Project Team of JAERI and KEK, JAERI-Tech 99-56, 1999.
2. Y. Ikeda, Nucl. Instrum. Meth. A600, (2009) 1.
3. Y. Miyake, et al., Physica B404 (2009) 957.
4. M. Futakawa, et al., J. Nucl. Sci. Technol.40 (2004)895.
5. M. Futakawa, et al., J. Nucl. Matter.343 (2005) 70.
6. S. Meigo, et al., ICANS-19 as presented as A051
7. S. Meigo, et al., Nucl. Instrum. Meth.A562, (2006) 569.
8. S. Sakamoto, et al., Nucl. Instrum.Meth.A562, (2006)638.